



## Room temperature versatile conversion of biomass-derived compounds by means of supported TiO<sub>2</sub> photocatalysts

Juan C. Colmenares\*, Agnieszka Magdziarz

*Institute of Physical Chemistry PAS, Kasprzaka 44/52, 01-224 Warsaw, Poland*

### ARTICLE INFO

#### Article history:

Received 12 September 2012

Received in revised form

17 September 2012

Accepted 17 September 2012

Available online 25 September 2012

#### Keywords:

Selective photocatalysis

Glucose photo-oxidation

Phenol aqueous degradation

TiO<sub>2</sub>

Sol-gel synthesis

Sonication

### ABSTRACT

The selective oxidation of glucose and degradation of phenol in liquid phase were studied in the presence of supported TiO<sub>2</sub> photocatalysts. Photocatalysts were synthesized by a modified ultrasound-assisted sol-gel method. The fact of supporting TiO<sub>2</sub> on zeolite type Y is giving more selective photocatalyst in glucose oxidation toward glucaric acid (GUA) and gluconic acid (GA) (total selectivity approx. 68%, after 10 min illumination time and 50% H<sub>2</sub>O/50% acetonitrile solvent composition) than the unsupported TiO<sub>2</sub> and the commercially available photocatalyst Evonik P-25. Photocatalysts worked at room temperature, atmospheric pressure and very short reaction times (up to 15 min). Additionally, these photocatalysts were investigated in the mineralization of phenol as a cellulosic industries water contaminant. It was observed that fumed silica is a better option than zeolite as titania support in phenol aqueous degradation.

Ultrasound-promoted sol-gel methodology is giving promising supported TiO<sub>2</sub> photocatalysts for water purification and solar chemicals production.

© 2012 Elsevier B.V. All rights reserved.

### 1. Introduction

Paper and pulp industry provides a significant amount of residues that constitute a renewable source of lignocellulosic material. This abundant, cheap and non-edible biomass replaced edible biomass feedstock (e.g. sugars, starches and edible oils) after the *food versus fuel* debate that emerged as a response to the sharp increase in food prices several years ago. Such replacement permitted sustainable production of fuels and chemicals without affecting food supplies or forcing extensive changes in land use [1]. Lignocellulose is a polymeric material composed of three primary units: cellulose (a crystalline polymer of glucose units), hemicellulose (an amorphous polymer of five different C<sub>5</sub> and C<sub>6</sub> sugars) and lignin (a three-dimensional polymer of propyl-phenol that surrounds cellulose and hemicellulose) [2].

In the cellulose-derived industries, phenols are among the most common contaminants that can be found in water and, due to their high toxicity, they are strictly regulated. Furthermore, their complete removal from water is relatively difficult because of their high stability in solution. Hence, photocatalysis has become a very promising method to eliminate such water organic pollutants [3]. Alternatively, in the same type of industries,

selective oxidation of cellulose-derived compounds can be driven by photocatalytic reactions providing high-value chemicals [4,5], among them the so-called platform molecules including a great variety of carboxylic acids (succinic, fumaric and malic acids, 2,5-furandicarboxylic, 3-hydroxypropionic, aspartic, glucaric, glutamic, itaconic, and levulinic acid) and many other building-block molecules (3-hydroxybutyrolactone, glycerol, sorbitol, and xylitol/arabitol) [6].

Heterogeneous photocatalysis employs semiconductor materials and among them titanium dioxide has been considered to be the most attractive due to its low cost, non-toxicity, strong oxidizing power, excellent photocatalytic activity and long-term photostability [7]. However, its main drawback is that it can only be activated under UV light irradiation ( $\lambda < 388$  nm) due to its large band gap energy, which restricts its application under the whole solar light spectrum [8]. To solve this problem, apart from other expensive and complicated procedures, ultrasound-promoted methodologies have been used to prepare visible-light active and well-crystallized mesoporous TiO<sub>2</sub> photocatalysts [9–11]. Moreover, there are several limitations to the use of “bare” TiO<sub>2</sub> in photocatalytic reactors, because of the fact that TiO<sub>2</sub> aggregates rapidly in suspension, resulting in smaller effective surface area and lower catalytic efficiency. The small size of TiO<sub>2</sub> particles also complicates the filtration of suspensions, making slurry photocatalytic reactors impractical [12]. Therefore, it has been suggested that fine TiO<sub>2</sub> particles should be anchored on supports for the ease of handling as well as to improve adsorption and photocatalytic efficiency [3].

\* Corresponding author. Tel.: +48 22 343 3215.

E-mail addresses: [jcarloscolmenares@ichf.edu.pl](mailto:jcarloscolmenares@ichf.edu.pl), [jcarlos@wp.pl](mailto:jcarlos@wp.pl) (J.C. Colmenares).

In this context, there have been numerous attempts to immobilize  $\text{TiO}_2$  catalyst on different supports as ceramic [13], silica [14,15], activated carbon [16,17], clay [18,19], and zeolite [20,21]. From this group, zeolites and silica distinguish themselves as supports due to their photocatalytically attractive features as good pollutant adsorption, diffusion properties and absence of light absorption [3]. Additionally, zeolites have been reported to delocalise band gap excited electrons of  $\text{TiO}_2$  and thereby minimize electron–hole recombination as if to favor photoinduced electron-transfer reactions [22].

In the present investigation,  $\text{TiO}_2$  supported on zeolite and silica materials has been synthesized for the first time by a modified sol–gel method assisted by ultrasonic irradiation. According to the chemical composition of lignocellulose, glucose as monomer of cellulose and phenol as representative water pollutant of the lignocellulosic industries have been chosen to serve as model compounds in liquid phase photocatalytic reaction tests: selective photocatalytic oxidation of glucose and phenol photocatalytic degradation.

## 2. Experimental

### 2.1. Preparation of photocatalysts

Titanium (IV) isopropoxide (TTIP, >98%, Acros Organics) was used as a precursor of titanium dioxide. Poly(ethylene) glycol (PEG, M.W. 400, Acros Organics) was used as a template direction reagent in photocatalysts preparation. D-glucuronic acid (>98%) was obtained from Alfa Aesar. Zeolite (CBV780, Y type) was purchased from Zeolyst International and silica (AEROSIL 200) was obtained from Evonik.

The catalysts were synthesized by a modified sol–gel method assisted by ultrasonic irradiation. Zeolite and silica supports were thermally treated at 450 °C during 8 h in static air before the synthesis procedure. A volume of 3.8 mL (12.5 mM, for a  $\text{TiO}_2$  nominal content of 15 wt% on each support) titanium (IV) isopropoxide was dissolved in 80 mL of 2-propanol at room temperature, 6 g of zeolite and 3 g of poly(ethylene glycol) were added and the mixture was treated with ultrasound (35 kHz, 560 W, Sonorex Digitec-RC, Bandelin) for 1 h in 5 and 10 min cycles (two times/5 min and five times/10 min, 2 min ultrasound off between cycles). Then, a mixture of 1.27 mM of D-glucuronic acid and 1.4 g of PEG (total ratio of PEG:Ti = 8:1) in water/2-propanol (25:47, v/v) was added using a programmable syringe pump (model NE-1000-E New Era Pump Systems Inc.) with the speed flow of 0.5 mL/min during ultrasonic treatment (10 min cycles with 2 min ultrasound off between cycles, the total time of this step was approx. 90 min). The final mixture was continuously exposed to ultrasound for 30 min, left aging at room temperature and magnetically stirred for 18 h, filtered through a G5 funnel, dried at 110 °C for 3 h and calcined in static air at 500 °C for 5 h. The resulting photocatalyst was designated as  $\text{TiO}_2/\text{Ze}$ .

According to the same procedure, silica supported  $\text{TiO}_2$  was synthesized, however a different amount of silica was used, 3 g, preserving the proportions among the chemicals. The sample was labeled as  $\text{TiO}_2/\text{SiO}_2$ . For comparative purposes, the results with the commercial photocatalyst Evonik P-25 and unsupported  $\text{TiO}_2$  (US) (synthesized by the same procedure) were also presented.

### 2.2. Photocatalytic tests

Glucose (ACS, pure p.a.) was purchased from POCH and phenol (99+%) was obtained from Alfa Aesar. Solvents and other

reagents were of analytical grade and used without any further purification.

All catalytic reactions were performed in a quartz (for glucose)/borosilicate glass (for phenol) cylindrical double-walled immersion well reactor with a total volume of 450 mL.

### 2.3. Case study #1: liquid-phase photocatalytic selective oxidation of glucose

The reaction system was stirred magnetically at 700 rpm to get a uniform suspension of the catalyst in the solution. A medium pressure 125 W mercury lamp ( $\lambda_{\text{max}} = 365 \text{ nm}$ ) supplied by Photochemical Reactors Ltd. (Model RQ 3010) was placed inside the quartz immersion well as light irradiation source. The reaction temperature was established at 30 °C. Glucose solutions (2.8 mM) were prepared in a mixture of Milli-Q water and acetonitrile (ACN) (10:90, v/v) unless otherwise specified. Experiments were carried out from 150 mL of mother solution and a concentration of 1 g/L of the catalyst was used. All reactions were carried out under ambient air (no oxygen bubbling conditions). Approx. 2 mL of samples were taken from the photoreactor at pre-specified periods of time and were filtrated (0.20  $\mu\text{m}$ , 25 mm  $\phi$  nylon filters) in order to remove  $\text{TiO}_2$ -supported particles before HPLC analyses.

The quantitative analyses for glucose selective conversion were measured, after calibration, by high-performance liquid chromatograph (Waters HPLC Model 590 pump), equipped with refractive index detector (Waters 2414 Refractive Index Detector). Separation was performed on a XBridge™ Amide 3.5  $\mu\text{m}$  4.6 mm  $\times$  150 mm Column provided by Waters. Mobile phase was MilliQ-water/acetonitrile (15:85, v/v) at a flow rate of 0.8 mL/min. The injection volume was 10  $\mu\text{L}$ .

All reaction products were identified by GC–MS (after silylation using N,O-bis(trimethylsilyl)trifluoroacetamide with 1% trimethylchlorosilane as derivatizing agent and performed at 60 °C for 1 h in a reactor CSB/COD-Reaktor ET 108, Aqualytic, Germany). All products identified by GC–MS were confirmed by LC/MS analysis. These analytical methods using both GC/MS and LC/MS were able to detect all intermediates (also for the case study #2 of phenol degradation).

Blank experiments were performed in the dark as well as with illumination and no catalyst, without observable change in the initial concentration of glucose in both cases.

### 2.4. Case study #2: liquid-phase photocatalytic degradation of phenol

All photocatalytic reactions with phenol were performed in the set-up described above (for the case study #1), however with a few modifications. The lamp was placed in a borosilicate glass immersion well (300 nm, wavelength at which a 1 mm layer of the glass absorbs at least 90% the light) in order to avoid autodegradation of phenol (an important phenol disappearance caused by photolysis under UV irradiation up to 300 nm was observed). Phenol solutions (50 ppm) were prepared in Milli-Q water. The reactions were carried out under ambient air. Phenol degradation was measured, after external standard calibration, by HPLC (Waters HPLC Model 590 pump), equipped with a PDA detector. Separation was performed on a XBridge™ C18 5  $\mu\text{m}$  4.6 mm  $\times$  150 mm column provided by Waters. The mobile phase was Milli-Q water/methanol (65:55, v/v) with 0.1% of  $\text{CF}_3\text{COOH}$  at a flow rate of 1 mL/min. The injection volume was 10  $\mu\text{L}$ .

The controlled experiments, without light or without photocatalyst, were performed to confirm that this reaction depends on the presence of both, light and photocatalyst.

**Table 1**  
Summary of the structural, textural and optical features concerning characterization of photocatalytic systems.

Catalyst	UV–vis		XRD		N <sub>2</sub> -isotherms		
	E <sub>gap</sub> (eV)	Absorption threshold (nm)	Crystallite <sup>a</sup> size (nm)	Crystal phase <sup>a</sup> (%)	S <sub>BET</sub> <sup>b</sup> (m <sup>2</sup> /g)	V <sub>p</sub> <sup>b</sup> (mL/g) <sup>a</sup>	r <sub>p</sub> <sup>b</sup> (Å)
Zeolite Y	–	–	–	–	784	0.52	27
SiO <sub>2</sub>	–	–	–	–	197	0.39	57
Evonik-P25	3.18	389	17.6 (A)/24.4 (R)	A (88)/R (12)	59	0.19	64
TiO <sub>2</sub> /Ze	3.27	379	7.9 (A)	A (100)	676	0.47	29
TiO <sub>2</sub> /SiO <sub>2</sub>	3.31	375	Not detectable	Not detectable	207	0.51	111

<sup>a</sup> A and R denote anatase and rutile, respectively.

<sup>b</sup> Specific surface area (S<sub>BET</sub>), cumulative pore volume (V<sub>p</sub>) and pore mean radius (r<sub>p</sub>).

## 2.5. Characterization of photocatalysts

The textural properties of photocatalysts were determined from N<sub>2</sub> adsorption–desorption isotherms at liquid nitrogen temperature by using a Micromeritics ASAP 2020 instrument. Surface areas and pore sizes were calculated by the Brunauer–Emmett–Teller (BET) and the Barret–Joyner–Halenda (BJH) methods, respectively. Prior to measurements, all samples were degassed at 110 °C to 0.1 Pa.

X-ray powder analysis was carried out with a XRD Siemens D5000 diffractometer using Ni-filtered CuK $\alpha$  radiation ( $\lambda = 1.5406 \text{ \AA}$ ) at 40 kV and 30 mA. The diffraction angle  $2\theta$  was scanned at a rate of  $2^\circ \text{ min}^{-1}$ . The average crystallite size of anatase was determined according to the Scherrer equation (Eq. (1)) using the full width at half maximum of the peak corresponding to 1 0 1 reflections and taking into account the instrument broadening.

$$D = \frac{K\lambda}{\beta \cos\theta} \quad (1)$$

where  $D$  is the average crystallite size of the catalyst (nm),  $\lambda$  is the wavelength of the Cu K $\alpha$  X-ray radiation ( $\lambda = 1.5406 \text{ \AA}$ ),  $K$  is a coefficient usually taken as 0.94,  $\beta$  is the full width at half maximum (FWHM) intensity of the peak observed at  $2\theta$  (radian), and  $\theta$  is the diffraction angle.

Ultraviolet–visible Diffuse Reflectance spectroscopy was performed using a UV-2501PC Shimadzu spectrophotometer. Band-gaps values were calculated based on the Kubelka–Munk functions,  $f(R)$ , which are proportional to the absorption of radiation, by plotting  $[f(R)h\nu]^{1/2}$  against  $h\nu$ . The function  $f(R)$  was calculated using Eq. (2) [23]:

$$f(R) = \frac{(1 - R)^2}{2R} \quad (2)$$

## 3. Results and discussion

### 3.1. Photocatalysts characterization

It is well-known that the amount of loaded TiO<sub>2</sub> in zeolite is significantly affected by structural parameters of zeolite such as SiO<sub>2</sub>/Al<sub>2</sub>O<sub>3</sub> ratio, cation type, and topology [24]. In this study, Y type zeolite, with the ratio SiO<sub>2</sub>/Al<sub>2</sub>O<sub>3</sub> = 80 and hydrogen (acidic) form has been chosen. The Y type zeolite exhibits the FAU (faujasite) structure is composed of tetrahedral SiO<sub>4</sub> and AlO<sub>4</sub> building blocks, which results in the formation of 3-dimensional pore structure material.

X-ray powder diffraction was used to determine the crystal phase of the catalyst particles. The XRD patterns of catalysts are shown in Table 1. The characteristic peak of anatase [1 0 1] phase at  $2\theta = 25.4^\circ$  has been observed for TiO<sub>2</sub>/Ze catalyst [25]. TiO<sub>2</sub> particle size calculated by means of Scherrer's equation was 7.9 nm for the nominal TiO<sub>2</sub> loading of 15 wt% (Table 1). Wang et al. [12] reported that the size of TiO<sub>2</sub> particles increases with increasing TiO<sub>2</sub> loading (28.9 nm. for 50 wt% of TiO<sub>2</sub>). He ascribed this

phenomenon to the aggregation of TiO<sub>2</sub> particles on the surface of the zeolite. Furthermore, it may suggest that in the case of catalyst with low TiO<sub>2</sub> loading, as in the studied case, the small amount of well-dispersed TiO<sub>2</sub> on the zeolite inhibits the mutual approach of fine TiO<sub>2</sub> particles, hence leading to the formation of crystals of finer size [12]. Also Zainudin et al. [26] report that the addition of barrier materials such as organic ligands, crystalline zeolites, porous amorphous polymers among others, can control the growth of the TiO<sub>2</sub> crystallites.

Peaks of anatase are not detectable on the XRD spectra of TiO<sub>2</sub>/SiO<sub>2</sub> catalyst. This observation can be explained by a high dispersion of TiO<sub>2</sub> particles on the SiO<sub>2</sub> surface or due to the very small TiO<sub>2</sub> clusters located within the silica pores [24]. However, the presence of TiO<sub>2</sub> in this sample can be deduced from the UV–vis spectrum that is presented in Fig. 1. As one can observe, a characteristic absorption peak ascribed to TiO<sub>2</sub> anatase phase is clearly seen for the TiO<sub>2</sub>/SiO<sub>2</sub> photocatalyst. Also, a blue-shift (to shorter wavelengths) is observed, and it represents a slight increase (Table 1 and Fig. 1) in the band gap energy value of supported TiO<sub>2</sub> in comparison with the bare TiO<sub>2</sub> (commercial Evonik P-25) from 3.18 to 3.3 eV., approximately. This can be explained by the quantum confinement effect of titania clusters within the supports texture and indicates that the size of titania nanoparticles in the zeolite and silica supports is smaller than that of P-25 [27]. A marked absorption of visible light in the range of 400–700 nm for TiO<sub>2</sub>/Ze (Fig. 1) was detected. Osorio et al. [28] prepared a visible-light responsive TiO<sub>2</sub> by low-frequency ultrasounds (LFUS) irradiation. Based on electron spin resonance (ESR) measurements, they found evidence for the formation of oxygen vacancies (V<sub>o</sub>) on this material, which were also found responsible for the visible-light absorption [28]. The V<sub>o</sub> surface defects might result from high-speed interparticle

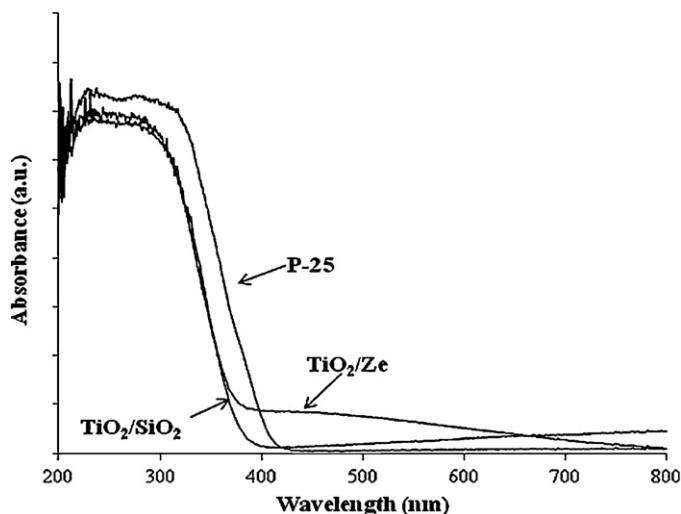


**Fig. 1.** Diffuse reflectance UV–visible spectra of catalyst samples: TiO<sub>2</sub>/Ze, TiO<sub>2</sub>/SiO<sub>2</sub> and Evonik P-25.

collisions and shock waves generated during the ultrasound-assisted sol–gel methodology used for supported TiO<sub>2</sub> photocatalyst synthesis. Further investigations are needed to confirm the presence of V<sub>o</sub> defects.

The pore volume and specific surface area of supported catalysts were determined using nitrogen adsorption–desorption isotherms and are presented in Table 1. Loading of TiO<sub>2</sub> on the zeolite surface results in the reduction of pore volume and surface area of zeolites (from 0.52 to 0.47 mL/g and from 784 to 676 m<sup>2</sup>/g, respectively). This can indicate that TiO<sub>2</sub> is dispersed on the zeolite surfaces and the pores of zeolite are partially blocked by TiO<sub>2</sub>. As the pore size of zeolite was smaller (<2.0 nm) than the size of the TiO<sub>2</sub> particles (approx. 7.9 nm) supported on the zeolite, the particles might not be deposited inside the pores of zeolite [13]. On the other hand, the surface area after loading of TiO<sub>2</sub> on the silica surface does not change significantly but the pore radius and volume changes are more evident. These changes may suggest an aggregation, in some cases under sonication [28], of TiO<sub>2</sub> particles on silica surface and the development of voids in this aggregation, which might create an additional pore volume [12].

### 3.2. Photocatalytic test reactions

#### 3.2.1. Case study #1: liquid-phase photocatalytic selective oxidation of glucose

In the photocatalytic oxidation of glucose three organic compounds have been obtained in the liquid phase, namely: glucaric acid (GUA), gluconic acid (GA) and arabitol (AOH). Carboxylic acids are very important building blocks for pharmaceutical, food, perfume and fuel industries. The arabitol component in the organic phase is also an important platform molecule [4,6] and it was detected only when 10% H<sub>2</sub>O/90% ACN solvent composition was used. Besides these liquid phase products, CO<sub>2</sub> and traces of hydrocarbons (methane, ethane, acetaldehyde) in gas phase have been detected. Scheme 1 presents a chart of the idea of the production of GUA and GA through a photocatalytic selective oxidation of glucose in liquid phase. As it can be observed in Scheme 1, all steps (except for step nr. 1) are very well known technologies of distillation (steps 3, 4, 7 and 8), filtration (step 2), drying (step 2) and reactive extraction of pure carboxylic acids (step 5), which guarantee good flexibility and effectiveness of producing high value carboxylic acids in a low-cost and environmentally friendly process.

Table 2 compares the selectivity results obtained for the studied photocatalysts for the first 10 min of photoreaction (this illumination time was chosen as it showed the best selectivity performance and difference among catalysts). As it is seen, zeolite-supported titania is the most selective in this time interval (total selectivity for GUA + GA is 68.1% with 15.5% glucose conversion). Moreover, the most popular photocatalyst P-25 showed several times lower carboxylic acids selectivity and higher glucose conversions (Table 2) than the catalysts prepared by the ultrasound-assisted sol–gel methodology. Unsupported TiO<sub>2</sub>(US) was giving lower glucose conversion and comparable selectivity to GUA and GA; at this point it is important to highlight the benefits of supporting TiO<sub>2</sub> (easy filtration) and the fact that for our catalysts, TiO<sub>2</sub> represents a nominal value of 15 wt% of the whole catalyst used in the reaction (150 mg of unsupported TiO<sub>2</sub> was applied), which makes supported photocatalysts more active and selective per gram of titania used. In the case of silica-supported titania the selectivity decreases more visibly in each time interval (results not shown), but the glucose conversion rate increases more rapidly (Fig. 2) in each solvent composition. Hence, the attribute of revealing better glucose degradation properties can be ascribed to titania supported on SiO<sub>2</sub>, while zeolite-supported titania showed better selectivity. Faster disappearance (Fig. 2) of glucose in the presence of silica-supported titania photocatalysts can be assigned to a larger amount or

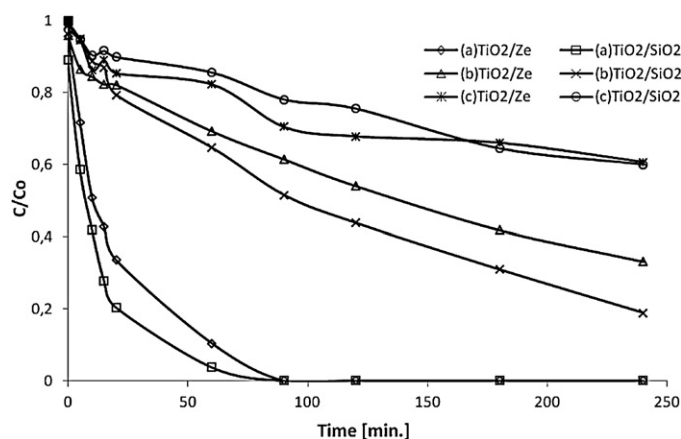


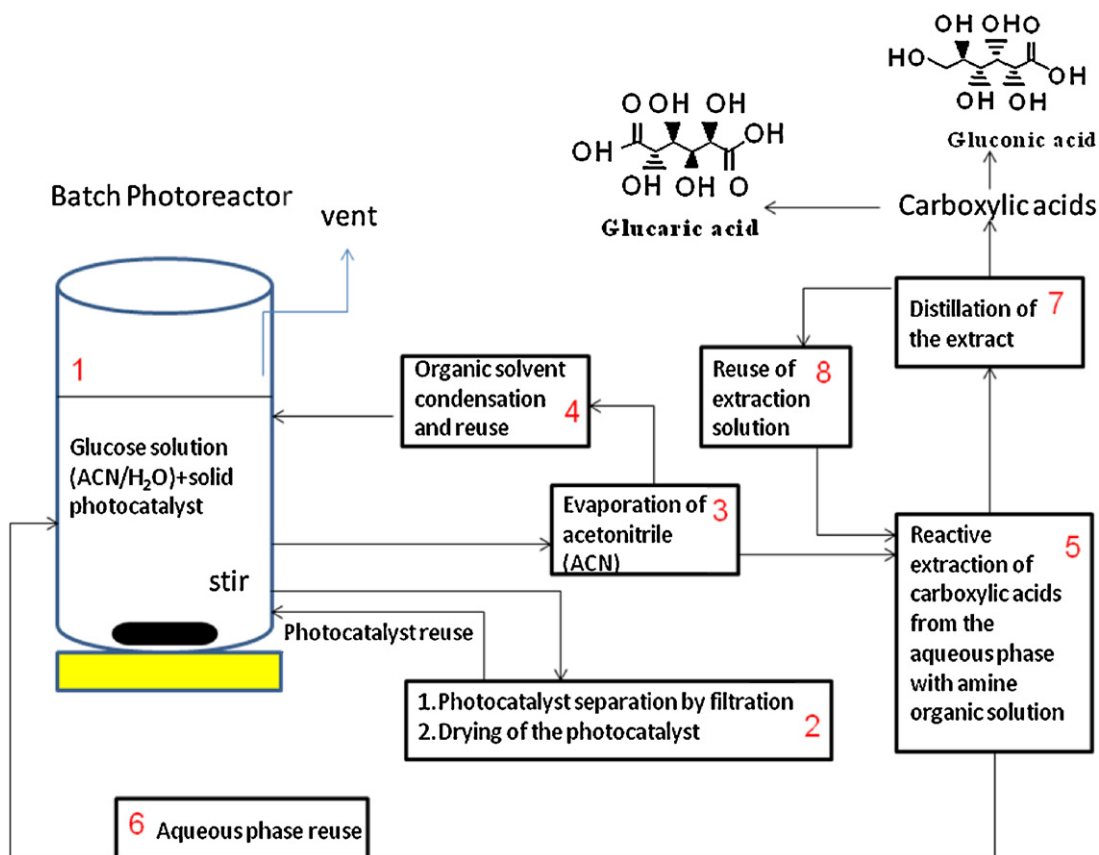
Fig. 2. Glucose disappearance for TiO<sub>2</sub>/Ze and TiO<sub>2</sub>/SiO<sub>2</sub> photocatalysts (reaction conditions: 150 mL of mother solution, C<sub>glucose</sub> = 2.8 mM, 150 mg of photocatalyst, temperature 30 °C, pressure 1 bar, solvent composition H<sub>2</sub>O:ACN: (a) 10:90, v/v (b) 50:50, v/v; (c) 100:0, v/v).

better distribution of active titania (anatase phase) sites on the silica surface.

The optimization of water/acetonitrile (ACN) reaction medium has also been investigated and the results are presented in Table 2. The presence of acetonitrile has been reported to improve selective photo-oxidation reactions [29]. It is clearly seen that the higher amount of water gives lower conversion (except for P-25 where the situation is the opposite). Herein, better photodegradation properties of silica-supported titania material are confirmed, as if in each H<sub>2</sub>O/ACN volume ratio glucose conversion on silica-supported titania is the highest (Fig. 2). The influence of H<sub>2</sub>O/ACN ratio on the selectivity has also been checked. No selectivity to carboxylic acids was observed for 100% H<sub>2</sub>O as solvent (Tab. 2). Interestingly, the selectivity to GUA and GA for 50% H<sub>2</sub>O/50% ACN solvent composition was improved (arabitol was not detected) under these conditions (64.8% and 68.1% for TiO<sub>2</sub>/SiO<sub>2</sub> and TiO<sub>2</sub>/Ze, respectively, Table 2). In this H<sub>2</sub>O/ACN volume ratio both photocatalysts are slightly more selective to gluconic acid (results not shown).

Controlling the photocatalytic degradation of target substrates in a selective way is a challenging issue since the reactivity of the hydroxyl radical is difficult to control [30]. Interesting properties of zeolites are negative charges (in our case balanced by counter protons present in zeolites pores) carried by the aluminosilicate framework, which results from the substitution of Al<sup>3+</sup> into the silica structure [31]. The electrostatic repulsion of anionic products (carboxylic acids) by the negatively charged zeolite framework facilitated the selective photocatalytic oxidation of glucose.

While the point of zero charge pzc (pzc describes the condition when electrical charge density on a surface is zero) of Evonik P-25 is approx. 6.5, those of TiO<sub>2</sub>/Ze could be significantly shifted to lower pH (approx. 2) [24] because of the negative charges of the zeolite framework. As a result, the surface of TiO<sub>2</sub>/Ze carries dominant negative charges at pH >2 (pH of the glucose solution before reaction is 6.3 ± 0.2, pKa (GA) = 3.35 and pKa (GUA) = 2.99) under these conditions carboxylic acids products should be repulsed preventing their total photo-oxidation. As it can be seen (Tab. 2), TiO<sub>2</sub>/Ze (better than TiO<sub>2</sub>/SiO<sub>2</sub>, TiO<sub>2</sub>(US) and much better than P-25) exhibits the charge-selective adsorption characteristics, which might affect the photocatalytic selectivity. Not only does the repulsion of carboxylic acids from TiO<sub>2</sub>/Ze surface (also observed for TiO<sub>2</sub>/SiO<sub>2</sub> and unsupported TiO<sub>2</sub>(US)) avoid their degradation but also their diffusion into the protective environment created by ACN (pKa = 25, as a weak base could stabilize the carboxylic acids by solvation and suppress their further oxidation), which demonstrates the important role of ACN especially for the solvent composition of 50% H<sub>2</sub>O/50% ACN.



**Scheme 1.** Chart of the concept of photocatalytic selective valorization of sugars (glucose) in liquid phase (H<sub>2</sub>O/ACN).

Shiraishi et al. [32] and Morishita et al. [33] demonstrated the positive influence of acetonitrile on formation of epoxides in the selective photo-oxidation of olefins. One more thing to highlight is the fact that the more acidic character of zeolite support in comparison to SiO<sub>2</sub>, unsupported TiO<sub>2</sub>(US) and Evonik P-25 could help in obtaining higher selectivity to carboxylic acids as it was found by An et al. [34]. They observed that the acidity of their tested catalysts (polyoxometalates-supported gold nanoparticles) not only favored the conversion of cellobiose in the presence of oxygen but also resulted in higher selectivity to gluconic acid by facilitating desorption and inhibiting its further degradation in aqueous phase.

TiO<sub>2</sub>/Ze visible light absorption (Fig. 1) could be ascribed to oxygen vacancies (V<sub>o</sub>) which might additionally induce the creation of surface photoactive centers in our hybrid material for a better photoselectivity in the formation of carboxylic acids from glucose oxidation (approx. 19% of the spectrum of the lamp used in photocatalytic tests was between 400 and 440 nm light wavelength). Further research will be focused on the demonstration whether or not V<sub>o</sub> defects are present on TiO<sub>2</sub>/Ze surface and also on the effect

of such defects on the selective photocatalytic oxidation of glucose through techniques such as electron spin resonance spectroscopy (ESR).

To sum up, all previous observations allowed us to conclude that the properties of TiO<sub>2</sub>, the nature of titania support and the reaction conditions (solvent composition, illumination time) play a key role in determining the photocatalytic behavior, particularly in determining the selectivity for GA and GUA.

### 3.2.2. Case study #2: liquid-phase photocatalytic degradation of phenol

Phenol disappearance, as a model reaction [35], was employed to investigate photocatalytic degradation properties of synthesized samples under UV irradiation. To verify the photocatalytic abilities of the samples, the experiments were conducted during 4 h of illumination. No appreciable phenol degradation was found in the absence of UV irradiation or catalyst. The concentration of phenol by photolysis decreased only to 11% after 4 h of illumination.

**Table 2**  
Effect of the solvent composition (water and acetonitrile ACN) on the conversion of glucose and selectivity to carboxylic acids for: TiO<sub>2</sub>/SiO<sub>2</sub>, TiO<sub>2</sub>/Zeolite, TiO<sub>2</sub>(US) and Evonik P-25 photocatalysts (reaction conditions: C<sub>glucose</sub> = 2.8 mM, 150 mL of mother solution, 150 mg of photocatalyst, temperature 30 °C, pressure 1 bar, 10 min illumination time).

Photocatalyst	Solvent composition					
	10%H <sub>2</sub> O/90%ACN		50%H <sub>2</sub> O/50%ACN		100%H <sub>2</sub> O	
	Conversion (%)	ΣSelectivity (%)	Conversion (%)	ΣSelectivity (%)	Conversion (%)	ΣSelectivity (%)
TiO <sub>2</sub> /SiO <sub>2</sub>	58.1	28.1	14.0	64.8	9.5	0.0
TiO <sub>2</sub> /Zeolite	49.2	29.5	15.5	68.1	13.7	0.0
TiO <sub>2</sub> (US)	28.8	27.3	11.0	71.3	41.2	0.0
Evonik P-25	60.4	12.1	67.3	8.5	78.8	0.0

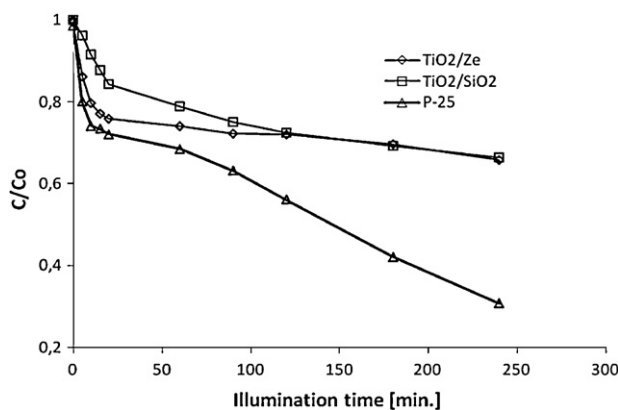


**Fig. 3.** Photocatalytic degradation of phenol in the presence of investigated catalysts: TiO<sub>2</sub>/Ze, TiO<sub>2</sub>/SiO<sub>2</sub>, and Evonik P-25 (reaction conditions: 150 mL of mother solution, 150 mg of photocatalyst, C<sub>phenol</sub> = 50 ppm prepared in Milli-Q water, temperature 30 °C, reaction pressure 1 bar).

Although upon approx. 100 min of illumination (Fig. 3) TiO<sub>2</sub>/Ze was more active than TiO<sub>2</sub>/SiO<sub>2</sub>, after 240 min of illumination the same phenol degradation rate is achieved for both photocatalysts (ca. 35% of degradation). It can be seen in Fig. 3 that the most active photocatalyst is Evonik P-25 with 69.3% of phenol degradation after 240 min of irradiation. Unfortunately, in the aqueous phase P-25 left, apart from phenol, the highest quantity of phenol-derived harmful compounds of negative effect on water quality (e.g. hydroquinone, catechol) among the investigated photocatalysts (TiO<sub>2</sub>/SiO<sub>2</sub> has shown negligible amount of these compounds, Fig. 4). HPLC–MS analyses (Fig. 4), upon 240 min of illumination time, showed intermediate by-products of partial photo-oxidation obtained in photocatalytic degradation of phenol evidencing a more selective mineralization to CO<sub>2</sub> and H<sub>2</sub>O in the presence of the photocatalysts prepared by the modified ultrasound-assisted sol–gel procedure (TiO<sub>2</sub>/SiO<sub>2</sub> > TiO<sub>2</sub>/Ze >> P-25, sequence of direct selectivity to complete mineralization).

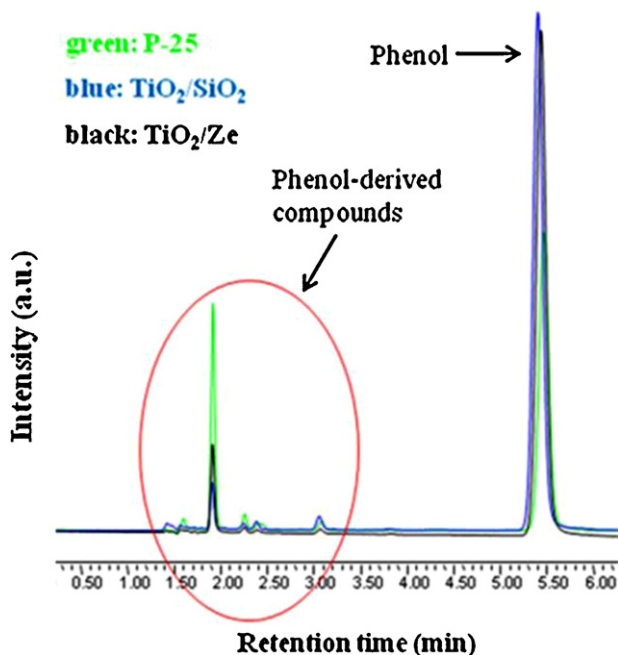


**Fig. 4.** HPLC–MS chromatographs for 240 min of photocatalytic degradation of phenol.

#### 4. Conclusions

Among the photocatalytic systems tested, the best performances in terms of organic products selectivity (GA + GUA) in glucose photocatalytic oxidation were especially remarkable in the case of the catalysts synthesized by the ultrasound-modified sol–gel method. TiO<sub>2</sub> supported on zeolite (TiO<sub>2</sub>/Ze) was the most selective toward glucaric/gluconic acid products (68.1% selectivity for a solvent composition of 50% H<sub>2</sub>O/50% ACN and 10 min of illumination). It was found that reactions conditions, especially solvent composition and short illumination times, also have considerable effect on the activity/selectivity of tested photocatalysts.

As far as phenol degradation is concerned, TiO<sub>2</sub>/SiO<sub>2</sub> is the best option as photocatalyst (ca. 35% of phenol disappearance for 240 min of illumination) because it is promoting mineralization of phenol to CO<sub>2</sub> and H<sub>2</sub>O with insignificant production (traces) of harmful and dangerous water contaminants (e.g. hydroquinone, catechol).

Studies on the selective photocatalytic conversion of glucose may provide important clues for the rational design of efficient photocatalysts for cellulose transformations and also for more effective photocatalysts in the fight against water pollutants.

#### Acknowledgments

This research was supported by a Marie Curie International Reintegration Grant within the 7th European Community Framework Programme. This scientific work was financed from the 2012–2014 science financial resources, granted for the international co-financed project implementation (Project Nr. 473/7.PR/2012, Ministry of Science and Higher Education of Poland). The authors express gratitude to Dr K. Noworyta for his help with the UV–vis Diffuse Reflectance measurements.

#### References

- J.C. Serrano-Ruiz, R. Luque, A. Sepulveda-Escribano, *Chem. Soc. Rev.* 40 (2011) 5266–5281.
- G. Centi, P. Lanzafame, S. Perathoner, *Catal. Today* 167 (2011) 14–30.
- M.V. Shankar, S. Anandan, N. Venkatachalam, B. Arabindoo, V. Murugesan, *Chemosphere* 63 (2006) 1014–1021.
- J.C. Colmenares, R. Luque, J.M. Campelo, F. Colmenares, Z. Karpinski, A.A. Romero, *Materials* 2 (2009) 2228–2258.
- J.C. Colmenares, A. Magdziarz, A. Bielejewska, *Bioresour. Technol.* 102 (2011) 11254–11257.
- (a) T. Werpy, G. Pedersen, *Top Value Chemicals from Biomass*, 1, US Department of Energy report, 2004; (b) J.J. Bozell, G.R. Petersen, *Green Chem.* 12 (2010) 539–554.
- M.A. Henderson, *Surf. Sci. Rep.* 66 (2011) 185–297.
- X. Chen, S.S. Mao, *Chem. Rev.* 107 (2007) 2891–2959.
- J.C. Yu, L. Zhang, J. Yu, *Chem. Mater.* 14 (2002) 4647–4653.
- J.C. Colmenares, M.A. Aramendia, A. Marinas, J.M. Marinas, F.J. Urbano, *Appl. Catal., A* 306 (2006) 120–127.
- S.Y. Kim, T.S. Chang, C.H. Shin, *Catal. Lett.* 118 (2007) 224–230.
- Ch.-C. Wang, C.-K. Lee, M.-D. Lyu, L.-Ch. Juang, *Dyes Pigments* 76 (2008) 817–824.
- F. Sunada, A. Heller, *Environ. Sci. Technol.* 32 (1998) 282–286.
- Y. Chen, K. Wang, L. Lou, J. Photochem. Photobiol. A 163 (2004) 281–287.
- Y. Xu, W. Zheng, W. Liu, J. Photochem. Photobiol. A 122 (1999) 57–60.
- J. Hermann, J. Matos, J. Disdier, C. Guillard, J. Laine, S. Malato, J. Blanco, *Catal. Today* 54 (1999) 255–265.
- H. Yoneyama, T. Torimoto, *Catal. Today* 58 (2000) 133–140.
- C. Ooka, H. Yoshida, K. Suzuki, T. Hattori, *Microporous Mesoporous Mater.* 67 (2004) 143–150.
- Z. Sun, Y. Chen, Q. Ke, Y. Yang, J. Yuan, J. Photochem. Photobiol. A 149 (2002) 169–174.
- M.G. Kang, H.S. Park, K.J. Kim, J. Photochem. Photobiol. A 149 (2002) 175–181.
- A. Bhattacharyya, S. Kawi, M.B. Ray, *Catal. Today* 98 (2004) 431–439.
- S. Sankararaman, K.B. Yoon, T. Yabe, J.K. Kochi, *J. Am. Chem. Soc.* 113 (1991) 1419–1421.
- S. Sakthivel, H. Kisch, *Angew. Chem. Int. Ed.* 42 (2003) 4908–4911.
- G. Zhang, W. Choi, S.H. Kim, S.B. Hong, *J. Hazard. Mater.* 188 (2011) 198–205.
- Y.H. Hsien, C.F. Chang, Y.H. Chen, S. Cheng, *Appl. Catal., B* 31 (2001) 241–249.
- N.F. Zainudin, A.Z. Abdullah, A.R. Mohamed, *J. Hazard. Mater.* 174 (2010) 299–306.

- [27] M.V. Rama-Krishna, R.A. Friesner, *J. Chem. Phys.* 95 (1991) 8309–8322.
- [28] P.A. Osorio-Vargas, C. Pulgarin, A. Sienkiewicz, L.R. Pizzio, M.N. Blanco, R.A. Torres-Palma, C. Pétrier, J.A. Rengifo-Herrera, *Ultrason. Sonochem.* 19 (2012) 383–386.
- [29] Y. Shiraishi, T. Hirai, *J. Photochem. Photobiol. C* 9 (2008) 157–170.
- [30] S.H. Zhan, D.R. Chen, X.L. Jiao, Y. Song, *Chem. Commun.* (2007) 2043–2045.
- [31] M.N. Chretien, *Pure Appl. Chem.* 79 (2007) 1–20.
- [32] Y. Shiraishi, M. Morishita, T. Hirai, *Chem. Commun.* (2005) 5977–5979.
- [33] M. Morishita, Y. Shiraishi, T. Hirai, *J. Phys. Chem. B* 110 (2006) 17898–17905.
- [34] D. An, A. Ye, W. Deng, Q. Zhang, Y. Wang, *Chem. Eur. J.* 18 (2012) 2938–2947.
- [35] V. Gomez, A.M. Balu, J.C. Serrano-Ruiz, S. Irusta, D.D. Dionysiou, R. Luque, J. Santamaria, *Appl. Catal., A* 441–442 (2012) 47–53.